



## Rapid Communication

## Homogenous high enhancement surface-enhanced Raman scattering (SERS) substrates by simple hierarchical tuning of gold nanofoams

Hanna J. Koster, Hannah J. O'Toole, Kwan Lun Chiu, Tatu Rojalin, Randy P. Carney\*

Biomedical Engineering, University of California, Davis, USA



## ARTICLE INFO

## Keywords:

Raman spectroscopy  
Plasmonics  
Nanomaterials  
Lithography  
Biosensor

## ABSTRACT

Surface enhanced Raman scattering (SERS) is a powerful tool for vibrational spectroscopy, providing orders of magnitude increase in chemical sensitivity compared to spontaneous Raman scattering. Yet it remains a challenge to synthesize robust, uniform SERS substrates quickly and easily. Lithographic approaches to produce substrates can achieve high, uniform sensitivity but are expensive and complex, thus difficult to scale. Facile solution-phase chemical approaches often result in unreliable SERS substrates due to heterogeneous arrangement of “hot spots” throughout the material. Here we demonstrate the synthesis and characterization of a homogeneous gold nanofoam (AuNF) substrate produced by a rapid, one-pot, four-ingredient synthetic approach. AuNFs are rapidly nucleated with macroscale porosity and then chemically roughened to produce nanoscale features that confer homogeneous and high signal enhancement ( $\sim 10^9$ ) across large areas, a comparable performance to lithographically produced substrates.

## 1. Introduction

Anisotropic metallic nanomaterials, including nanorods, nanowires, nanostars, nanourchins, and nanofoams, have gained traction in a wide variety of applications due to their unique chemical and physical properties [1]. These versatile materials exhibit high chemical stability and biocompatibility and can be readily tuned for enhanced near-infrared (NIR) optical absorption with large extinction cross-sections. As such, they have been broadly applied in catalysis [2], electrochemistry [3], and sensing of chemical warfare agents or environmental pollutants [4]. Uses in biomedical platforms as photothermal agents, drug delivery carriers, and biosensing materials [5–7] have also been shown.

Compared with other anisotropic nanomaterials, applications of nanofoams have lagged, in part due to their synthetic and structural complexity compared to particle formulations. Nanofoams are porous nanomaterials typically created from copper [8], silver [9], or gold [10,11]. They are most commonly fabricated by chemical etching of biphasic mixtures of metals in the presence of strong acids that de-alloy the sample, leaving behind a porous phase [12]. Other fabrication methods employ biopolymers in combination with autoclave heat treatments to form networks after hydrothermal synthesis [13], or use halide ions to induce aggregation of gold nanoparticles (AuNPs) to form

3D networks [14]. More complex methods utilize electrodeposition and sintering [15]. Each of these has various limitations, either relying on dangerous precursors with high environmental hazards (e.g., concentrated nitric acid [12]), or feature complex procedures resulting in nanofoams that are difficult to structurally tune. For example, control over pore size and tortuosity is important for biosensing applications, such as simultaneous point-of-use filtration and sensing via optical readout, yet current methods are unable to easily tune these parameters [12].

A central application of nanofoams where precise synthetic control is needed for effective biosensing readout is surface-enhanced Raman scattering (SERS). SERS is an attractive biosensing tool, as it is non-destructive, label-free, highly sensitive, provides a detailed chemical fingerprint of the sample, and is not influenced by water, meaning it can be performed in aqueous solutions such as wastewater or complex human biofluids [16]. SERS is an ultrasensitive extension of inherently weak spontaneous Raman scattering, whereby Raman signal originating from molecules in the near field of nanoscale anisotropic metallic architectures are dramatically enhanced by many orders of magnitude [16]. A SERS/Raman spectrum is comprised of peaks corresponding to numerous vibrational and rotational modes arising from a given chemical sample, providing sensitive and specific information about which molecules are present [17]. This information has been broadly applied

\* Corresponding author at: Department of Biomedical Engineering, University of California, Davis, Davis, CA 95616, USA.

E-mail address: [rcarney@ucdavis.edu](mailto:rcarney@ucdavis.edu) (R.P. Carney).

<https://doi.org/10.1016/j.colcom.2022.100596>

Received 21 December 2021; Received in revised form 27 January 2022; Accepted 28 January 2022

Available online 17 February 2022

2215-0382/© 2022 The Authors.

Published by Elsevier B.V. This is an open access article under the CC BY-NC-ND license

(<http://creativecommons.org/licenses/by-nc-nd/4.0/>).

in biosensing to detect and diagnose diseases, such as cancer [18], cardiovascular diseases [19], and neurological diseases [20] as well as other applications such as environmental sensing and food testing [21].

One of the main obstacles to clinical translation of SERS is the nature of commonly used substrates, the best of which are typically created with expensive, specialized lithography equipment to pattern delicate nanostructures onto microscale planar surfaces [16]. It remains a grand challenge to rapidly and cost-effectively synthesize highly tunable hierarchically-ordered macroscale substrates with nanoscale SERS active features. Current tactics to generate such materials employ large-scale solution-phase synthesized anisotropic nanomaterials like nanorods and nanourchins deposited onto surfaces to form SERS active substrates [22]. Other shapes such as nanostars [23], nanocubes [24], and nanotriangles [25], typically made from silver, have also been used. Yet these approaches are difficult to reproduce, often synthetically complex (necessitating several steps of inorganic chemical reactions and purification), and do not result in tortuous materials (e.g., foams) that could be used for in-line filtration. Additionally, nanoparticle deposition on planar surfaces often results in heterogeneous drying patterns with large spot-to-spot enhancement variation. Quantitative analysis of

analytes using heterogeneous substrates is challenging since one cannot readily determine whether signal-intensity fluctuations are a result of analyte concentration or rather distribution and quality of “hot spots” on the substrate. There is a need to develop solution-phase synthesized macroscale nanofoams comprised of plasmonic metals for homogeneous SERS activity and sensing.

To address this gap, here we introduce a new gold nanofoam (AuNF) material with nanoscale features endowing high, homogeneous SERS enhancement and with a tunable porous structure for potential in-line filtration and sensing applications. These AuNFs are easily synthesized via a rapid, one-pot, four-ingredient mixture at room temperature, and then concurrently purified and integrated into a stable filter by simple drop drying. Critically, our new synthetic scheme (Fig. 1) allows for control over the macro-, micro-, and nano-scale features. Highly tunable microscale pore sizes are controlled by modulating the starting concentration of the two starting ingredients, a gold salt, and a citrate reducing agent. Nanoscale roughening is achieved via a subsequent gold deposition step and sonication. Macroscale structure is achieved by drop-drying as-synthesized AuNFs onto a paper filter. The resulting roughened nanofoam (RNF) assembly has high and homogeneous

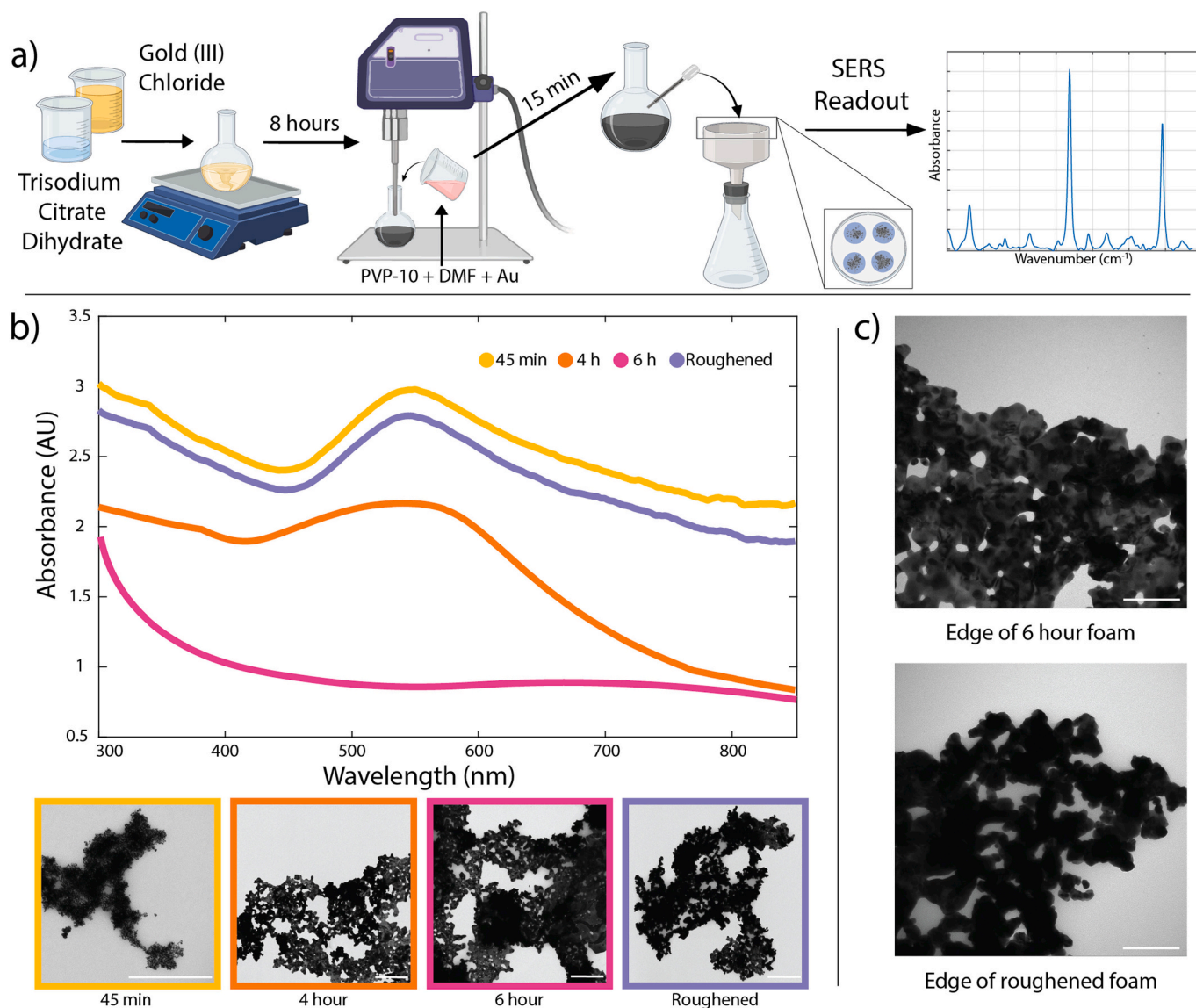


**Fig. 1.** a) Overview of hierarchically tuned nanofoam synthesis and deposition onto filter paper. b) UV-vis spectra and corresponding TEM images of nanofoams at time points 45 min, 4 h, 6 h, and after chemical roughening. Scale bar is 500 nm for all images. c) TEM images of the edges of normal foams at the 6 h timepoint (top) and roughened nanofoams (bottom), scale bar 100 nm.

Raman enhancement factors approaching and even surpassing lithographically produced commercial substrates.

## 2. Experimental

### 2.1. Materials

Gold (III) chloride trihydrate (HAuCl<sub>4</sub>), trisodium citrate dihydrate, adenine, 4-mercaptobenzoic acid (4-MBA), poly (vinylpyrrolidone), MW = 10,000, (PVP-10), melamine, ethanol (EtOH), and *N,N*-dimethylformamide (DMF) were purchased from Sigma Aldrich and used without any further modifications. Milli-Q (MQ) water (resistivity = 18.2 MW cm<sup>-1</sup>) was used for all preparations.

### 2.2. Nanofoam synthesis

Gold nanofoams (AuNFs) were fabricated by mixing trisodium citrate dihydrate and HAuCl<sub>4</sub> reactants at differing molar ratios of ( $R = C_{\text{citrate}}/C_{\text{gold}}$ ). Initial experiments were carried out with  $R = 12$  on a stir plate following rinsing with EtOH and drying under air. 31 mg of HAuCl<sub>4</sub> was added to 32 mL of ultrapure water in a 50-mL round bottom flask with consistent magnetic stirring maintained at 550 rpm. 367.5 mg of trisodium citrate dihydrate was added directly to the flask while stirring. The reaction proceeded at room temperature under constant stirring. The yellow solution quickly turned clear followed by darkening to a purple/black within an hour of the reaction start. Aliquots were taken from the solution at 2 h and 5 h, and the reaction was stopped at 8 h. By this point, AuNFs had precipitated out of solution to form visible black masses at the bottom of the flask, and the solution became clearer. Foams were collected by gentle decantation or left in the flask for subsequent roughening procedure.

### 2.3. Nanofoam roughening

For roughening, the AuNFs were produced as above, except at the 6 h mark, excess volume was removed until 5 mL of the original solution (containing dispersed AuNFs) remained in the flask. A separate solution of 7 mL DMF, 0.1875 g PVP-10, and 40  $\mu$ L of 50 nM HAuCl<sub>4</sub> (in MQ water) was made and added to the original nanofoam mixture. The flask was clamped and an ultrasonication probe (Sonics & Materials INC., CT, USA) inserted into the solution while avoiding touching any of the glass. The mixture was sonicated for 15 min at 30% power (power = 130 W, frequency = 20 kHz) at which point a noticeable blue color shift occurred in the solution. Resulting roughened nanofoams (RNFs) were used in downstream assays as is with no further purification.

### 2.4. UV-Vis spectroscopy

Absorption spectra were collected using the NanoDrop One (Thermo Fisher) with a path length of 1 mm. 2  $\mu$ L samples dispersed in MQ water were pipetted onto the readout platform, and subsequent measurements were taken.

### 2.5. Electron microscopy

Scanning electron microscopy (SEM) images were obtained using a Thermo-Fisher Quattro S (ThermoFisher Scientific, Waltham, MA, USA) to visualize AuNF surface morphology. The instrument is equipped with an Everhart-Thornley detector (ETD) for secondary electron imaging. Prior to imaging, filters were sputtered with 5 nm gold to reduce substrate charging from the electron beam. Substrates were then mounted on metal studs using two-sided black carbon tape, and the following typical imaging parameters were applied: working distance 10.0 mm, spot size 3.0, accelerating voltage 10.0 or 15.0 kV. Transmission electron microscopy (TEM) images were obtained on a Talos L120C (Thermo Fisher Scientific, MA, USA). 2  $\mu$ L of nanofoam solution was dropped onto

copper formvar carbon support grids and allowed to dry before imaging.

### 2.6. Raman spectroscopy

All spectra were collected using a custom-built inverted Raman scanning confocal microscope with excitation wavelength of 785 nm and a 60 $\times$ , 1.2 NA water immersion objective on an inverted IX73 Olympus microscope. An Andor Kymera-3281-C spectrophotometer and Newton DU920P-BR-DD CCD camera were used for Raman spectra capture and Solis v4.31.30005.0 software was used for initial processing. The pinhole size was set to 1 mm, allowing operation in essentially *epi* collection mode with an increased depth of field. Careful focusing was carried out for each sample to ensure the bulk of the substrate is centrally located in the focal volume. For measurements, raster scans were performed as 20  $\times$  20 pixels with a 400 nm step size equalling an 8  $\mu$ m by 8  $\mu$ m area. Heat maps were generated by selecting a pronounced spectral feature with a normalized color scale. Five scans of 400 spectra (i.e., 20  $\times$  20 pixels) were performed on each substrate and averaged. Analysis of the spectral data was performed using MATLAB v2021a (MathWorks, MA, USA) via a custom script. Briefly, spectra were background and baseline corrected.

### 2.7. Nanofoam deposition to form filters

Following the synthetic procedure, as-prepared nanofoam solutions were dropped using a Pasteur pipette onto 13 mm, 0.22  $\mu$ m pore size, hydrophilic PVDF Durapore filter paper (MilliporeSigma) placed in a ceramic Büchner funnel under vacuum. Build-up of nanofoams was achieved by continuous dropping before allowing to completely dry. Adequate surface coverage was achieved after 75 drops of AuNF solution, determined by creating filters with increasing numbers of drops (in increments of 25 up to 100 drops) and then measuring SERS signal at random spots throughout the substrate. SEM images of the surface coverage with corresponding pictures of the filters can be seen in Fig. S1. The Raman standard melamine was used as a test molecule due to SERS specific peaks that are only visible when the plasmon resonance is high enough. The emergence of enhanced signal across large areas of the substrate, as suggested by a measurable increase in reporter analyte signal, indicated sufficient AuNFs structure to generate SERS (Fig. S2). Subsequent filters were made with at least 75 drops of our reaction.

## 3. Results and discussion

We developed the AuNF synthesis scheme (Fig. 1a) using a one-pot aqueous chemical reaction, mixing gold (III) chloride with trisodium citrate dihydrate in a round bottom flask at room temperature, as adapted from a recent report [11]. The effective microscale pore size and nanostructures could be tuned by varying the molar ratios of the two reagents ( $R = C_{\text{citrate}}/C_{\text{gold}}$ ). Typical experiments used an  $R = 12$  ratio of citrate to gold. Due to the slow reduction of the gold salt by the moderate citrate reducing agent, several intermediate structures are formed over the course of 6 h, each of which can be isolated by quenching the reaction via centrifugation and subsequent washing in ultra-pure water (Fig. 1b). The reaction starts as a pale-yellow color that turns clear within a few seconds of stirring. After  $\sim$ 45 min the solution turned gray and an intermediate structure resembling nanotadpoles is obtained [11]. After 4 h, integrated nanowire networks form as tadpoles coalesce. As the reaction proceeds to 6 h, the gold structures continue to grow and fuse, finally creating a three-dimensional nanofoam structure. UV-VIS spectra were obtained at each of the intermediate time points to track the AuNF evolution (Fig. 1b). As the foams continue to grow, they lose the nanostructures that give rise to the characteristic absorbance peak (520 nm) and gain more broad features indicative of elongated rods and wires. After  $\sim$ 8 h highly porous black foams precipitate out of the solution, which can be isolated by decanting the liquid and drying it under air.

While the emergence of microscale porosity during nanofoam evolution gives rise to useful and desired tortuosity, the nanoscale dimensions that enable SERS enhancement coarsen and thus are lost. To re-roughen the AuNFs, a solution of PVP-10 and gold (III) chloride in DMF was prepared and added to the AuNF seed solution at the 6 h mark (when foam networks were developed but not yet precipitated), and then probe ultrasonicated until the solution turned blue (~15 min). This color change indicates the presence of urchin-like features, forming a new material we refer to as roughened nanofoams (RNFs) (Fig. 1c).

AuNFs or RNFs were each deposited dropwise onto filter paper to form a substrate of several packed layers of foams. Scanning electron microscopy (SEM) images indicate the emergence of clear nanoscale features on the foams (Fig. 2), showing the effectiveness of our chemical roughening procedure. Further, we measured the reappearance of the AuNP absorbance peak using UV-VIS spectroscopy (Fig. 1b) indicating that the smaller nanostructures that give rise to SERS enhancement are once again ubiquitous throughout the substrate.

We compared the SERS activity of AuNFs with RNFs using the common reporter molecule 4-mercaptobenzoic acid (4-MBA) [26]. Filters for each substrate were generated and incubated with a solution of 4-MBA. We chose 4-MBA as a Raman standard because of the well-characterized interaction of its terminal thiol group with gold surfaces, which provides a straightforward method to approximate the surface coverage of our substrates [26]. At least 100 SERS spectra collected across several spots on each filter were collected, averaged, and used to compute the SERS enhancement factor (EF) by using the equation:

$$EF = \frac{I_{SERS}}{N_{SERS}} \times \frac{N_{RS}}{I_{RS}}$$

where  $I_{SERS}$  is the SERS signal of a chosen frequency,  $I_{RS}$  is the

spontaneous Raman signal at that same frequency,  $N_{SERS}$  is the number of molecules excited in SERS and  $N_{RS}$  is the number of molecules excited in spontaneous Raman (i.e., 4-MBA measured under the identical optical conditions but without any foams) [26].

Fig. 3 shows representative SERS spectra (Fig. 3a) for the AuNFs and RNFs, where it is apparent that the RNFs are highly homogeneous from spot to spot. Fig. 3b-3e plot the SEM images and spectral maps at the chosen  $I_{SERS}$  frequency of  $1077\text{ cm}^{-1}$  for the AuNF and RNF substrates, as well as two commercially produced substrates (Ocean Optics and Hamamatsu). EFs were calculated by estimating  $N_{SERS}$  according to the percentage of SERS active surface, using the topological surface area by SEM analysis and the molecular surface area of 4-MBA (see Supplemental Information). RNFs exhibited an impressive EF of  $2.0 \times 10^9$  compared to AuNF EF of  $7.3 \times 10^8$ . Hamamatsu substrates had an EF of  $4.0 \times 10^9$  and Ocean Optics substrates an EF of  $5.8 \times 10^9$ . Hence, the RNFs show a 2.7-fold magnitude increase compared to the AuNF and comparable EF to lithographically fabricated commercial substrates. Rasterized Raman scanning reveals that the RNFs exhibit high spot-to-spot homogeneity of SERS signal across its surface (Fig. 3c), besting commercial gold nanoparticle (Fig. 3d) and lithographically fabricated substrates (Fig. 3e). To assess the NF stability and shelf life, we tested foams four months after synthesis, which had been stored at room temperature. We were able to achieve the same degree of homogeneous EF signals from these scans (Fig. S4).

Together, this data demonstrates that the additional chemical sharpening did indeed increase the EF (and EF homogeneity) of RNFs. PVP is a crucial player in the sharpening process from AuNFs to RNFs. PVP-10 is used in this process as both the capping and stabilization agent for sharpening the rounded AuNF precursor features. In general, reduction of gold salts by PVP can be tuned by varying PVP concentration to control the reaction kinetics of reduction of  $\text{AuCl}_4^-$  ions to atomic gold atoms, which subsequently cap the surface of the gold

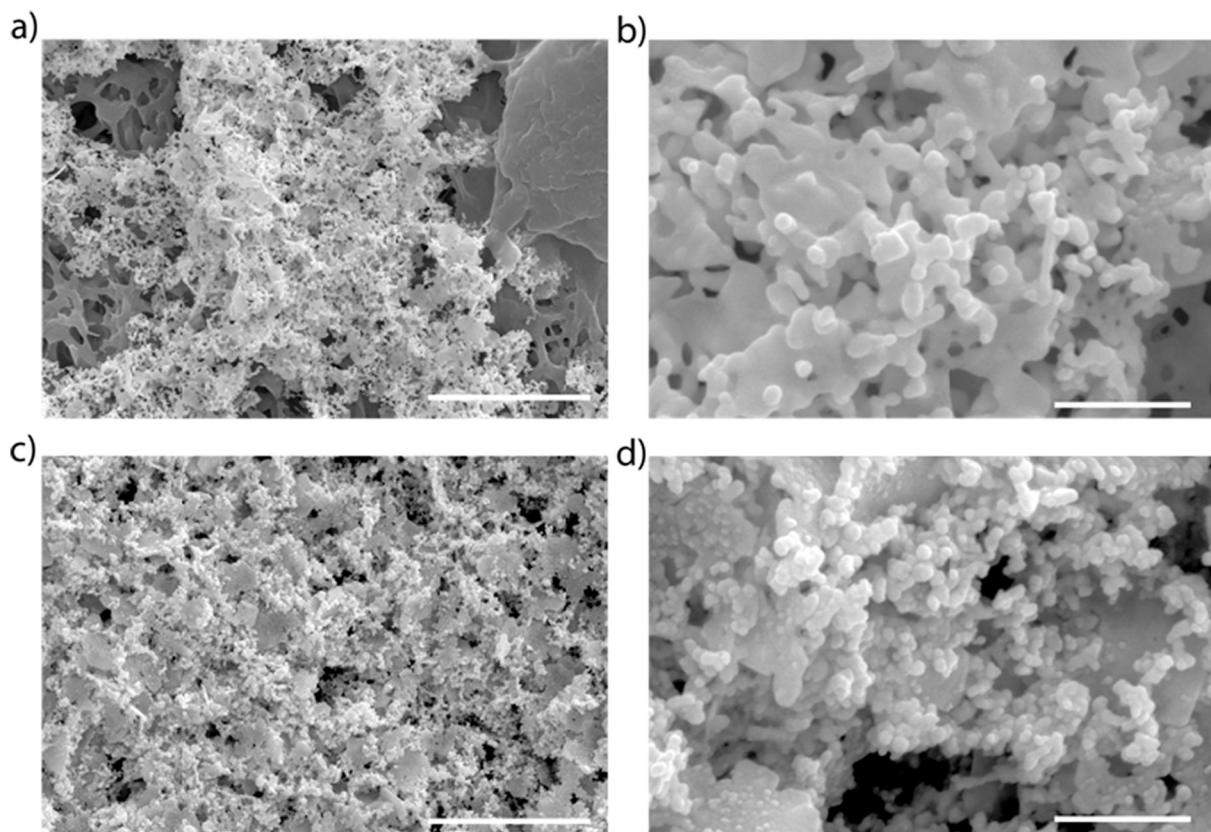
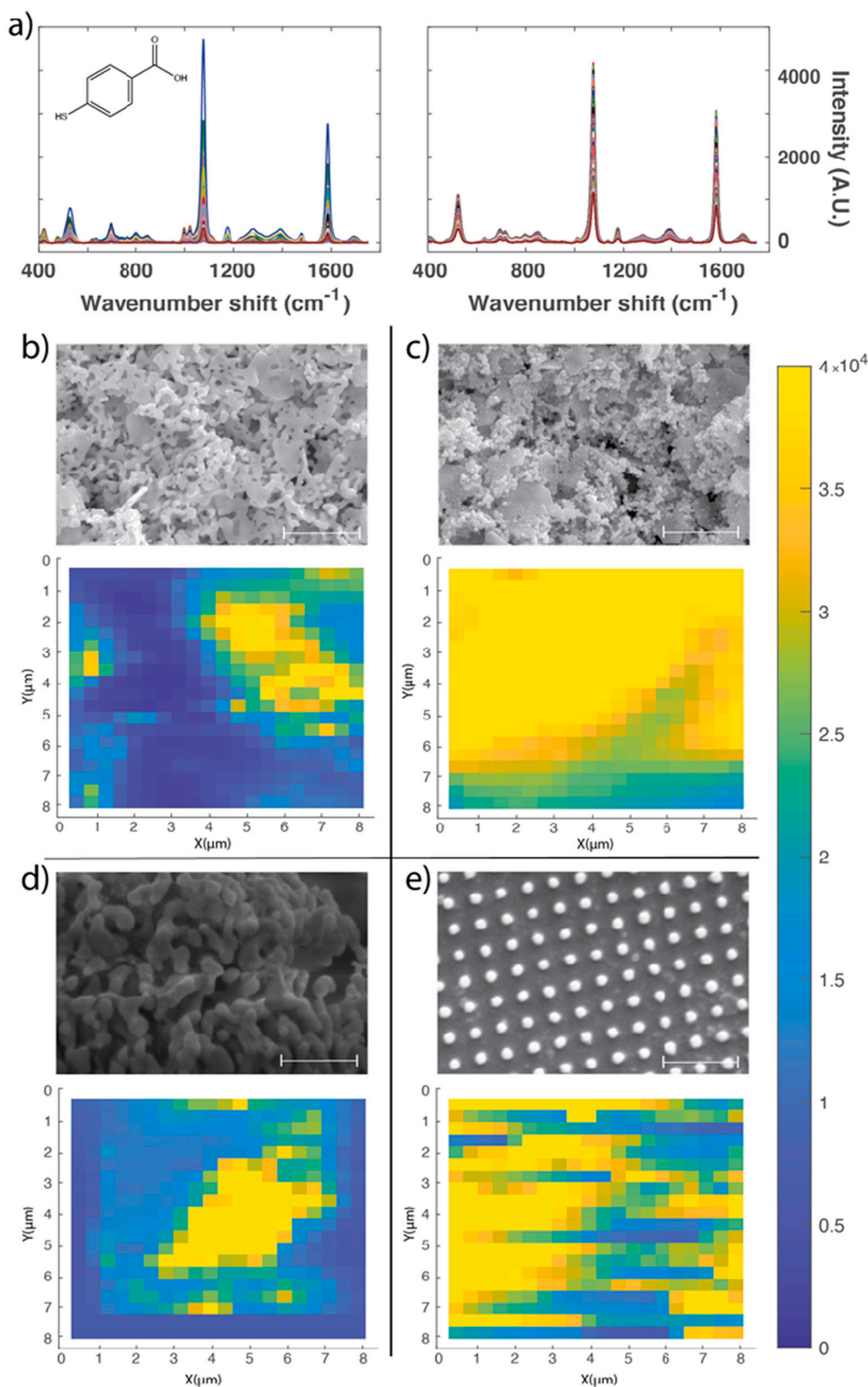


Fig. 2. SEM images of (a,b) 6 h AuNFs and (c,d) RNFs at magnifications of 20kx (left panels, scale bar is 4  $\mu\text{m}$ ) and 100kx (right panels, scale bar is 500 nm). Following chemical roughening, the emergence of high density, ~20–50 nm nanoscale features is apparent.



**Fig. 3.** Raman scanning of various SERS substrates with 4-MBA. Each raster scan represents an  $8 \mu\text{m}$  by  $8 \mu\text{m}$  area with a step size of  $400 \text{ nm}$ . a) Representative spectra of 4-MBA for AuNFs (left) and RNFs (right). SEM image and raster scan intensity at  $1077 \text{ cm}^{-1}$  for b) AuNFs, c) chemically roughened RNFs, and commercial d) Ocean Optics and e) Hamamatsu SERS substrates. All scale bars are  $1 \mu\text{m}$ .

nanofoams at the poorly passivated  $\{111\}$  faces [27,28]. This process enables the formation of anisotropic gold features desirable for SERS enhancement [28]. We hypothesized that incorporating PVP-mediated sharpening as previously used to sharpen gold colloids into rod-like,

or urchin-like morphologies [28], would similarly sharpen our AuNFs. Thus, the AuNF “seeds” were sonicated in a one-pot solution with PVP solubilized in DMF along with  $\text{HAuCl}_4$ . We optimized PVP concentration to allow for surface passivation at non-preferred facets while minimizing

spontaneous generation of AuNPs in solution. This is the first report of using PVP-mediated sharpening to roughen AuNFs.

Finite-difference time-domain (FDTD) simulation was performed to further evaluate the SERS EF provided by the AuNFs and RNFs [29]. The topological structure of the substrates as obtained by the SEM imaging (Fig. 4) was used as the model for 3D construction. Local E field was calculated via FDTD simulation at the wavelength of 785 nm used in this work. EF was approximated as  $\left(\frac{E}{E_0}\right)^4$  where E is the local electric field and  $E_0$  is the input source electric field [30]. Since standard SEM is limited in resolving 3D morphological structure, an alternative topological model more closely aligned with the morphological nature of the AuNFs and RNFs was generated within a 500 nm × 500 nm simulation region, approximating the focal volume of optical measurement (see Supplemental Information). Here, RNFs exhibit a significantly higher average enhancement factor compared to AuNFs, which agrees with the experimental results.

There is a gap in SERS substrates that are easy and inexpensive to synthesize, while also having high performance in enhancement and spot-to-spot homogeneity. These RNFs address this gap and will have value in point-of-use, disposable sensing applications. For example, due to their tortuous nature, they could be used for in-line fluidic analysis, and easily disposed of after use. We envision that automation of this simple synthesis process and filter development will allow fast, robust, and ready-to-use SERS substrates that provide sensitive readout of different samples—from environmental pollutants in water samples to potential chemical biomarkers in cancerous biofluids.

#### 4. Conclusions

In this study, we generated porous AuNFs and developed a

straightforward chemical roughening approach to further improve the nanostructure with respect to SERS enhancement. The resulting RNFs provided an increased EF with sensitive chemical SERS readout while increasing the signal homogeneity and providing a larger number of consistent hotspots throughout the material. These inexpensive and easily fabricated RNFs are comparable in EF to more expensive and complex lithographically produced commercial SERS substrates. Our results are an exciting step in the direction of increasing the efficacy of SERS biosensing by generating simple, robust, and reproducible SERS materials that may be applied to point-of-use sensing applications.

#### Data availability

The datasets generated during and/or analyzed during the current study are available in a Zenodo repository with the identifier <https://doi.org/10.5281/zenodo.5911304>. MATLAB code used to process datasets generated and/or analyzed during the current study are available from the corresponding author on request.

#### Funding sources

This work was supported by the National Institutes of Health [R01CA241666]; the UC Davis Comprehensive Cancer Center; the UC Davis Center for Data Science and Artificial Intelligence Research (CeDAR); and the Ovarian Cancer Education and Research Network, Inc. (OCERN). The ThermoFisher Quattro ESEM was funded through the US National Science Foundation under award DMR-1725618. H.J.O. was supported by the training grant T32GM136597 from the National Institutes of Health.

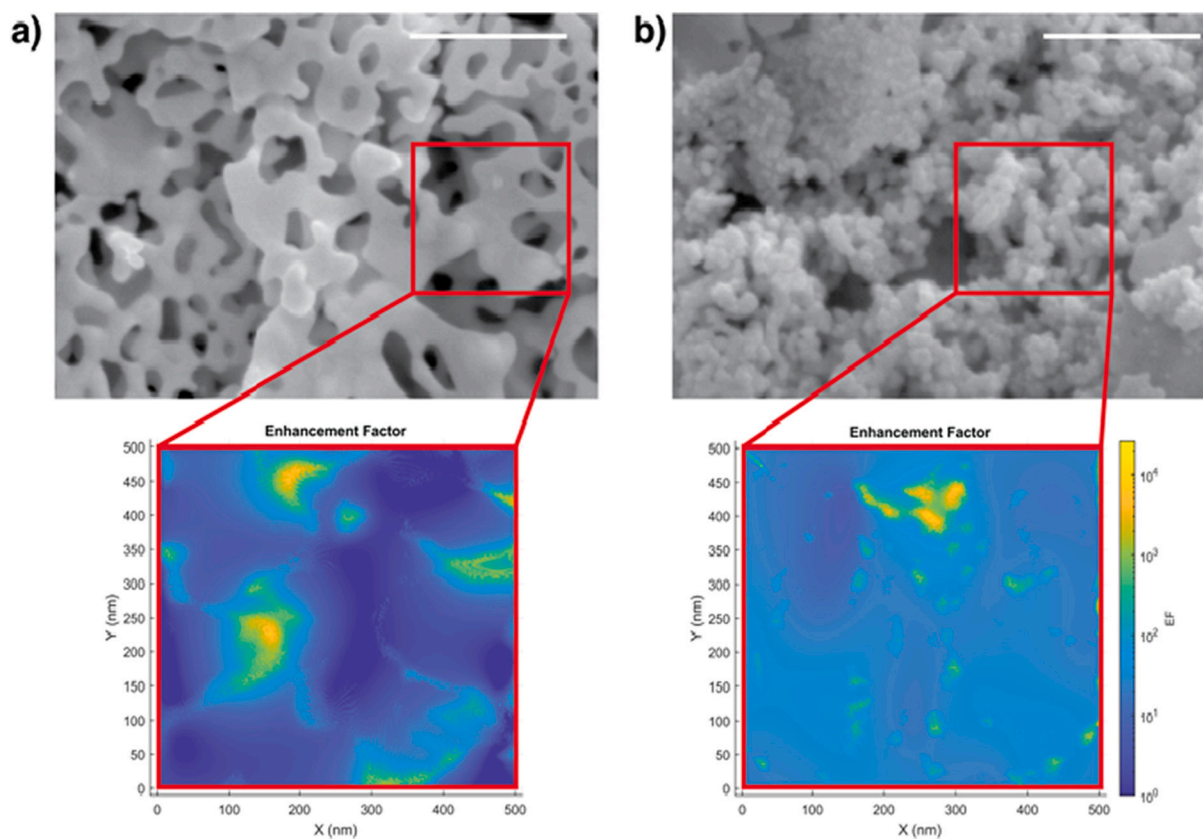


**Fig. 4.** FDTD simulation of electromagnetic enhancement. Topological features extracted from SEM images of AuNFs (a) and RNFs (b) were used to model the local EF of the substrates. RNFs feature a homogeneously increased EF throughout the substrate (insets represent roughly the optical focal area during scanning). Scale bar = 500 nm.

## CRedit authorship contribution statement

**Hanna J. Koster:** Conceptualization, Methodology, Investigation, Writing – original draft, Visualization. **Hannah J. O’Toole:** Conceptualization, Investigation, Writing – review & editing. **Kwan Lun Chiu:** Methodology, Formal analysis, Visualization, Writing – review & editing. **Tatu Rojalín:** Methodology, Formal analysis, Visualization, Writing – review & editing. **Randy P. Carney:** Conceptualization, Supervision, Funding acquisition, Project administration, Writing – review & editing.

## Declaration of Competing Interest

The authors declare that they have no known competing financial interests or personal relationships that could have appeared to influence the work reported in this paper.

## Appendix A. Supplementary data

The following files are available free of charge. 1. Buildup of nanofoams on filters; Raman of melamine on filters; SERS analysis of 4-month old RNFs; Calculation of SERS enhancement factor; SERS surface area modeling and nanostructure analysis; Simulation of optical properties for nanofoams; SEM images of model AuNF structures. Supplementary data to this article can be found online at [<https://doi.org/10.1016/j.colcom.2022.100596>].

## References

- [1] G. Paramasivam, N. Kayambu, A.M. Rabel, A.K. Sundramoorthy, A. Sundaramurthy, Anisotropic noble metal nanoparticles: synthesis, surface functionalization and applications in biosensing, bioimaging, drug delivery and theranostics, *Acta Biomater.* (February 1, 2017) 45–65, <https://doi.org/10.1016/j.actbio.2016.11.066>. Elsevier Ltd.
- [2] A. Wittstock, J. Biener, M. Bäumer, Nanoporous gold: a new material for catalytic and sensor applications, *Phys. Chem. Chem. Phys.* 12 (40) (2010) 12919–12930, <https://doi.org/10.1039/c0cp00757a>.
- [3] K. Rong, L. Huang, H. Zhang, J. Zhai, Y. Fang, S. Dong, Electrochemical fabrication of nanoporous gold electrodes in a deep eutectic solvent for electrochemical detections, *Chem. Commun.* 54 (64) (2018) 8853–8856, <https://doi.org/10.1039/C8CC04454F>.
- [4] F. Dong, R.T. Koodali, H. Wang, W.K. Ho, Nanomaterials for environmental applications, *J. Nanomater.* 2014 (2014), <https://doi.org/10.1155/2014/276467>.
- [5] J. Veselinovic, S. Almashtoub, E. Seker, Anomalous trends in nucleic acid-based electrochemical biosensors with nanoporous gold electrodes, *Anal. Chem.* 91 (18) (2019) 11923–11931, <https://doi.org/10.1021/ACS.ANALCHEM.9B02686>.
- [6] F. Scaglione, E. Alladio, A. Damin, F. Turci, C. Baggiani, C. Giovannoli, S. Bordiga, L. Battezzati, P. Rizzi, Functionalized nanoporous gold as a new biosensor platform for ultra-low quantitative detection of human serum albumin, *Sensors Actuators B Chem.* 288 (2019) 460–468, <https://doi.org/10.1016/J.SNB.2019.03.005>.
- [7] X.-Y. Lang, H.-Y. Fu, C. Hou, G.-F. Han, P. Yang, Y.-B. Liu, Q. Jiang, Nanoporous gold supported cobalt oxide microelectrodes as high-performance electrochemical biosensors, *Nat. Commun.* 4 (1) (2013) 1–8, <https://doi.org/10.1038/ncomms3169>, 2013 41.
- [8] H. Lim, D. Kim, Y. Kim, T. Nagaura, J. You, J. Kim, H.J. Kim, J. Na, J. Henzie, Y. Yamauchi, A mesopore-stimulated electromagnetic near-field: electrochemical synthesis of mesoporous copper films by micelle self-assembly, *J. Mater. Chem. A* 8 (40) (2020) 21016–21025, <https://doi.org/10.1039/D0TA06228F>.
- [9] H. Lim, D. Kim, G. Kwon, H.J. Kim, J. You, J. Kim, M. Eguchi, A.K. Nanjundan, J. Na, Y. Yamauchi, Synthesis of uniformly sized mesoporous silver films and their SERS application, *J. Phys. Chem. C* 124 (43) (2020) 23730–23737, [https://doi.org/10.1021/ACS.jpcc.0c07234/SUPPL\\_FILE/JP0C07234\\_SI\\_001.PDF](https://doi.org/10.1021/ACS.jpcc.0c07234/SUPPL_FILE/JP0C07234_SI_001.PDF).
- [10] B.C. Tappan, A.S. III Steiner, E. Dervishi, A.H. Mueller, B.L. Scott, C. Sheehan, E. P. Luther, J.P. Lichthardt, M.R. Dirmyer, Monolithic nanoporous gold foams with catalytic activity for chemical vapor deposition growth of carbon nanostructures, *ACS Appl. Mater. Interfaces* 13 (1) (2020) 1204–1213, <https://doi.org/10.1021/ACSAMI.0C17624>.
- [11] A. Jakhmola, M. Celentano, R. Vecchione, A. Manikas, E. Battista, V. Calcagno, P. A. Netti, Self-assembly of gold nanowire networks into gold foams: production, ultrastructure and applications, *Inorg. Chem. Front.* 4 (6) (2017) 1033–1041, <https://doi.org/10.1039/c7qi00131b>.
- [12] V. Zielasek, B. Jürgens, C. Schulz, J. Biener, M.M. Biener, A.V. Hamza, M. Bäumer, Gold catalysts: nanoporous gold foams, *Angew. Chem. Int. Ed.* 45 (48) (2006) 8241–8244, <https://doi.org/10.1002/anie.200602484>.
- [13] S. Gao, H. Zhang, X. Wang, J. Yang, L. Zhou, C. Peng, D. Sun, M. Li, Unique gold sponges: biopolymer-assisted hydrothermal synthesis and potential applications as surface-enhanced Raman scattering substrates, *Nanotechnology* 16 (11) (2005) 2530, <https://doi.org/10.1088/0957-4484/16/11/012>.
- [14] Z. Zhiqiang, et al., Investigation of halide-induced aggregation of Au nanoparticles into spongelike gold, *Langmuir* 30 (10) (2014) 2648–2659, <https://doi.org/10.1021/LA4046447>.
- [15] J. Malloy, A. Quintana, C.J. Jensen, K. Liu, Efficient and robust metallic nanowire foams for deep submicrometer particulate filtration, *Nano Lett.* 21 (7) (2021) 2968–2974, <https://doi.org/10.1021/ACS.NANO.1C00050>.
- [16] D. Eustace, D. Graham, G. McNay, K. Faulds, W.E. Smith, Surface-enhanced Raman scattering (SERS) and surface-enhanced resonance Raman (SERRS): a review of applications, *Appl. Spectrosc.* 65 (8) (2011) 825–837, <https://doi.org/10.1366/11-06365>. Vol. 65, Issue 8, pp. 825–837.
- [17] S.I.R.C.V. Raman, Part 11.-The Raman Effect, 1929, pp. 781–792.
- [18] L. Guerrini, R.A. Alvarez-Puebla, Surface-enhanced Raman spectroscopy in cancer diagnosis, prognosis and monitoring, *Cancers (Basel)* 11 (6) (2019) 625–633, <https://doi.org/10.3390/CANCERS11060748>.
- [19] X. Fu, Y. Wang, Y. Liu, H. Liu, L. Fu, J. Wen, J. Li, P. Wei, L. Chen, A graphene oxide/gold nanoparticle-based amplification method for SERS immunoassay of cardiac troponin I, *Analyst* 144 (5) (2019) 1582–1589, <https://doi.org/10.1039/c8an02022a>.
- [20] A. Zengin, U. Tamer, T. Caykara, A SERS-based sandwich assay for ultrasensitive and selective detection of Alzheimer’s tau protein, *Biomacromolecules* 14 (9) (2013) 3001–3009, <https://doi.org/10.1021/bm400968x>.
- [21] D. Zhang, H. Pu, L. Huang, D.W. Sun, Advances in flexible surface-enhanced Raman scattering (SERS) substrates for nondestructive food detection: fundamentals and recent applications, *Trends Food Sci. Technol.* 109 (2021) 690–701, <https://doi.org/10.1016/J.TIFS.2021.01.058>.
- [22] F. Xu, W. Shang, G. Ma, Y. Zhu, M. Wu, Metal organic framework wrapped gold nanourchin assembled on filter membrane for fast and sensitive SERS analysis, *Sensors Actuators B Chem.* 326 (2021), 128968, <https://doi.org/10.1016/J.SNB.2020.128968>.
- [23] Shuai He, Jefri Chua, E.K. Ming Tan, J.C. Yong Kah, Optimizing the SERS enhancement of a facile gold nanostar immobilized paper-based SERS substrate, *RSC Adv.* 7 (27) (2017) 16264–16272, <https://doi.org/10.1039/C6RA28450G>.
- [24] W.A. Tegegne, W.N. Su, A.B. Beyene, W.H. Huang, M.C. Tsai, B.J. Hwang, Flexible hydrophobic filter paper-based SERS substrate using silver nanocubes for sensitive and rapid detection of adenine, *Microchem. J.* 168 (2021), 106349, <https://doi.org/10.1016/J.MICROC.2021.106349>.
- [25] C. Wang, B. Liu, X. Dou, Silver nanotriangles-loaded filter paper for ultrasensitive SERS detection application benefited by interspacing of sharp edges, *Sensors Actuators B Chem.* 231 (2016) 357–364, <https://doi.org/10.1016/J.SNB.2016.03.030>.
- [26] S.E.J. Bell, G. Charron, E. Cortés, J. Kneipp, M.L. de la Chapelle, J. Langer, M. Procházka, V. Tran, S. Schlücker, Towards reliable and quantitative surface-enhanced Raman scattering (SERS): from key parameters to good analytical practice, *Angew. Chem. Int. Ed.* 59 (14) (2020) 5454–5462, <https://doi.org/10.1002/anie.201908154>.
- [27] P. Senthil Kumar, I. Pastoriza-Santos, B. Rodríguez-González, F. Javier García De Abajo, L.M. Liz-Marzán, High-yield synthesis and optical response of gold nanostars, *Nanotechnology* 19 (1) (2008) 1–7, <https://doi.org/10.1088/0957-4484/19/01/015606>.
- [28] M. Tsuji, M. Hashimoto, Y. Nishizawa, M. Kubokawa, T. Tsuji, Microwave-assisted synthesis of metallic nanostructures in solution, *Chem. A Eur. J.* 11 (2) (2005) 440–452, <https://doi.org/10.1002/CHEM.200400417>.
- [29] H. Jung, M. Park, M. Kang, K.-H. Jeong, Silver nanoislands on cellulose fibers for chromatographic separation and ultrasensitive detection of small molecules, *Light Sci. Appl.* 5 (1) (2016), <https://doi.org/10.1038/lsa.2016.9>, 2016 51. e16009–e16009.
- [30] E.C. Le Ru, P.G. Etchegoin, Rigorous justification of the |E|<sup>4</sup> enhancement factor in surface enhanced Raman spectroscopy, *Chem. Phys. Lett.* 423 (1–3) (2006) 63–66, <https://doi.org/10.1016/J.CPLETT.2006.03.042>.